Journal of Colloid and Interface Science 636 (2023) 549–558

Contents lists available at ScienceDirect

Journal of Colloid and Interface Science

journal homepage: www.elsevier.com/locate/jcis

Microfluidic jet impact: Spreading, splashing, soft substrate deformation and injection

Diana L. van der Ven [a], Davide Morrone [b], Miguel A. Quetzeri-Santiago [a,1,*], David Fernandez Rivas [a,*]

[a] Mesoscale Chemical Systems group, MESA+ Institute and Faculty of Science and Technology, University of Twente, P.O. Box 217, 7500 AE Enschede, the Netherlands
[b] Nanovea SRL, Via Balegno 1, 10040 Rivalta di Torino, Italy

GRAPHICAL ABSTRACT

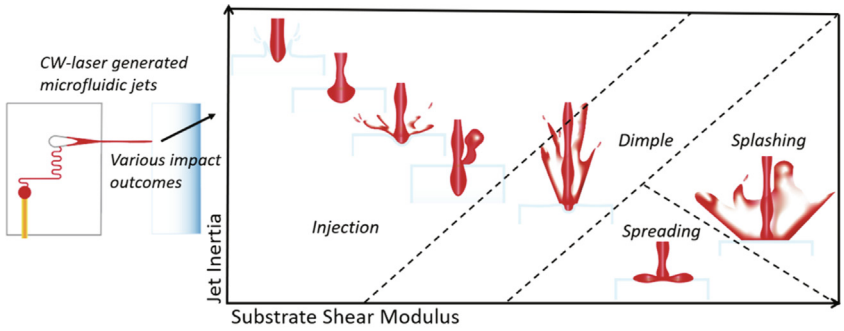

ARTICLE INFO

Article history:
Received 26 October 2022
Revised 3 January 2023
Accepted 5 January 2023
Available online 9 January 2023

Keywords:
Needle-free injections
Jet impact
Splashing
Spreading
Deformation
Microfluidics

ABSTRACT

Hypothesis: Needle-free injections using microfluidic jets could be optimized by reducing splashing and controlling injection depth. However, this is impeded by an incomplete understanding on how jet characteristics influence impact outcome. We hypothesise that exploring the relation between microfluidic jet characteristics and substrate shear modulus on impact behavior will assist in predicting and giving insights on the impact outcome on skin and injection endpoints.

Experiments: To do so, a setup using microfluidic chips, at varying laser powers and stand-off distances, was used to create thermocavitation generated microfluidic jets with ranging characteristics (velocity: 7–77 m/s, diameter: 35–120 μm, Weber-number: 40–4000), which were impacted on substrates with different shear modulus.

Findings: Seven impact regimes were found, depending on jet Weber-number and substrate shear modulus, and we identified three thresholds: i) spreading/splashing threshold, ii) dimple formation threshold, and iii) plastic/elastic deformation threshold. The regimes show similarity to skin impact, although the opacity of skin complicated determining the threshold values. Additionally, we found that jet velocity has a higher predictive value for injection depth compared to the Weber-number, and consequently, the jet-diameter. Our findings provide fundamental knowledge on the interaction between microfluidic jets and substrates, and are relevant for optimizing needle-free injections.

1. Introduction

Solid needle injections have inherent drawbacks despite their wide use and effectiveness in medical and cosmetic procedures.

* Corresponding authors.
E-mail addresses: m.a.quetzerisantiago@utwente.nl (M.A. Quetzeri-Santiago), d.fernandezrivas@utwente.nl (D. Fernandez Rivas).
[1] Current address: Department of Engineering Science, University of Oxford, Oxford OX1 3PJ, United Kingdom.

https://doi.org/10.1016/j.jcis.2023.01.024
0021-9797/

Worldwide, 16 billion needles are disposed yearly [1], with an additional 12 billion due to the COVID-19 vaccinations [2], creating an environmental burden in terms of material usage and waste [3,4]. Needles pose infection risks upon sticking incidents [5] and re-use, the latter being estimated to cause over 500 million deaths yearly [6]. Additionally, injections cause pain, and fear is experienced by 22% of the adult population [7]. This fear may result in avoidance of treatment [8,9], thereby decreasing the effectiveness of vaccination programs [10]. To address these issues, alternatives to conventional injections are being developed, such as liquid jet injections. Liquid jets can be made by accelerating fluids with various mechanisms [11–13]. Most commercialized injectors can only perform injections at a minimum depth of $\approx$ 1 mm, and are associated with pain and bruising, limiting their appeal in replacing needles [14,15].

Controlled, superficial, jet injections into the epidermis may result in reduced tissue damage, causing less bruising and pain compared to the current alternatives [16–19]. Moreover, control over injection depth could improve the pharmacokinetics of various therapeutics. For example, vaccines delivered within the epidermis require five to ten times less dosing due to the abundance of specialized immune cells [20,21]. Also, dermal insulin injections are reported to be more efficient compared to traditional subcutaneous delivery [22].

The relation between jet characteristics and injection depth in the skin must be understood to enable controlled injections. Correlating input parameters with the injection depth can be challenging as skin is a highly complex, multilayered tissue [23]. The mechanical response of skin is dependent on measurement type, leading to reported skin stiffness values ranging from 20 kPa – 1 GPa [24,25]. Additionally, the skin layers contribute differently to the mechanical behavior, with the stratum corneum and epidermis reported to be significantly stiffer compared to the dermis [24,26]. Nevertheless, an average lower limit of 20 kPa is often used reference [27,26]. Additionally, skin's poro-viscoelastic behavior causes a portion of the injected liquid to be ejected during, or after, injection, due to the elastic recovery of the material (squeeze-out) [28–31].

Multiple papers show how jet parameters relate to injection depth [15,28,32,33], dispersion of injected liquid within the substrate[28,33–35], and delivery efficiency [17,28,33]. However, a detailed study of the impact behavior, especially the break-up of a jet upon impact (splashing) and squeeze-out, at the microscale is lacking. Splashing and squeeze-out should be prevented or reduced, as both decrease delivery efficiency, and pose infection risks in extreme cases [36,37]. Preventing or reducing splashing requires knowledge about microfluidic jet impact behavior and how this relates to jet break-up. Droplet splashing has been extensively characterized [38–48], and it has been shown to depend on the substrate, liquid characteristics, and ambient pressure [38,39,49,50]. Furthermore, it is known that microscale droplets show different impact behavior compared to macroscale droplets, as the rim of liquid formed after the impact becomes comparable to the mean free path of air molecules [51–53]. In contrast to droplet splashing, studies on jet impact and splashing are limited, and reported values for the splashing threshold vary widely [54,55]. Furthermore, few studies have explored the splashing dynamics for substrates with different storage moduli [56,30,57], and it remains unknown how microscale jet behavior compares to macroscale jets.

Therefore, in this paper, we study microfluidic jet impact and injection behavior onto a range of substrate stiffness to gain fundamental knowledge on fluid dynamics and soft matter response. This knowledge can assist in optimizing controlled needle-free injections by controlling injection depth, and reducing splashing and squeeze-out. Furthermore, we make a qualitative comparison between observed phenomena on the impact on skin and the impact on agarose gels and glass.

2. Materials and methodology

2.1. Methodology

A continuous wave (CW) laser setup was employed to perform controlled injections with microfluidic jets using thermocavitation. A vapor bubble is created upon CW laser beam exposure at the glass-liquid interface due to the conversion of laser energy to heat [58,59]. The bubble expands and pushes the liquid out of the chip as a liquid jet. The process is depicted in Fig. 1. By changing the channel design, the channel filling level, the input laser power, laser pulse duration, and distance from the laser focal point to the base of the chip, jets with varying characteristics can be obtained [18,27]. Three channel designs were used to generate jets with ranging properties. Chip1 generates low velocity jets (7–37 m/s) due to the lack of a tapered nozzle [18,60,27]. The tapering is present on chip2 resulting in higher velocities (17–67 m/s) [18,60,61]. Additionally, chip3 increases the maximum jet speed (77 m/s) due to the curved channel wall [18]. (see Table 1).

2.2. Experimental setup

The experimental setup consists of a glass microfluidic chip filled with a water-dye solution and a CW laser diode (λ = 450 nm) focused on the glass-liquid interface using a 10x objective (Olympus) (see Fig. 1). An Arduino controller sets the laser pulse duration (10–30 ms) [18]. The chips were designed and fabricated from MEMPax Borofloat glass wafers (Schott) under cleanroom conditions [27]. The chips are aligned with the substrates at a stand-off distance of X_s = 2 mm. X_s is defined as the space in-between the nozzle and substrate surface, as illustrated in Fig. 1. To exclude any influence of X_s on impact outcome it is kept constant across experiments. The substrates used and relevant properties are shown Table 2, details on substrate preparation and characterization can be found at the Supplemental subsection: Agarose gel characterization. A red dye (Direct Red 81, Sigma, CAS: 2610–119) was dissolved at 0.5 wt% in deionized water (dH_2O) to maximize the laser energy absorption of the liquid. The solution had a density, ρ = 1000 kg/m^3; viscosity, η = 0.91 mPaS; and surface tension, σ = 47mN/m, as determined at 22°C and described elsewhere [18]. Due to the absorption coefficient ($\alpha = 100cm^{-1}$) [18] and cavitation times (20 ms) of our system, the liquid properties of the jet are not affected by heating [62], as further explained in supplemental subsection: Jet liquid properties.

Nucleation, jetting, impact and injection events are imaged using a high-speed camera (Photron FASTCAM SA-X2) with a mounted Navitar (12x Ultra Zoom) at 2x magnification captured at 1.8×10^5 or 1.2×10^5 frames per second (fps), and backlight illuminated using a SCHOTT light source (CV-LS series) with flexible light guide. The field of view was either 640×128 or 768×64 pixels with a pixel size of 10 μm. A mounted long pass 495 nm filter (Thorlabs, FGL495M) was used to avoid over saturation from the laser light. By performing image analysis of the high-speed images V_{jet} (travelled distance over time), D_{jet} (width of jet-tip prior to impact) and impact duration (defined as the time between the start and end of jet impact) are measured.

3. Results and discussion

The large range of jets showed distinct impacting behavior depending on jet and substrate characteristics. We observed seven

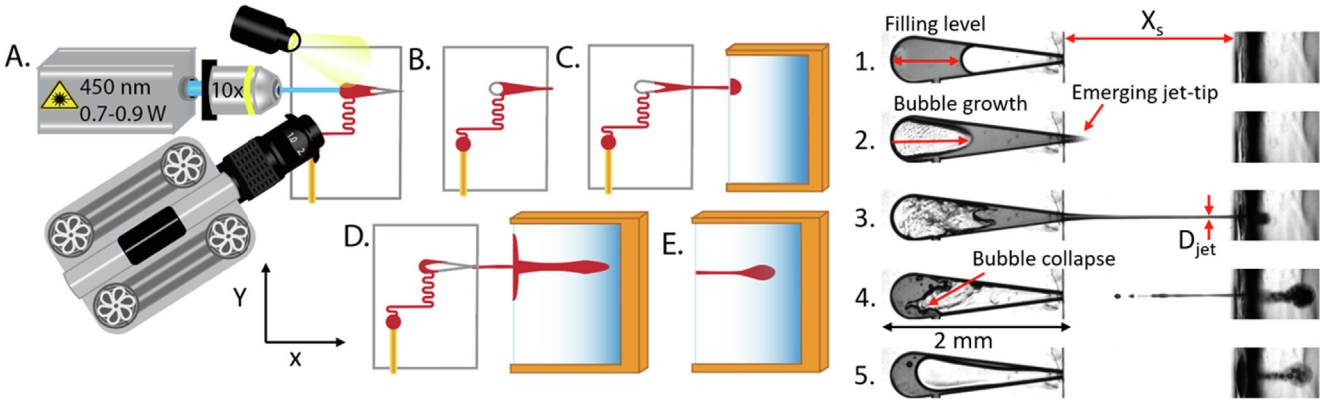

Fig. 1. Left) Depiction of setup for angular movies (for side shots the camera is perpendicular to the chip). The CW laser is focused on the base of the chip chamber (A), and heats the liquid inside the chamber, generating an expanding bubble (B). This bubble pushes the liquid in front of it and generates a microfluidic jet (B - C). The jet impacts the substrate surface (C), and injects if the impact velocity is larger than the threshold value (D). Afterwards, the formed cavity contracts (E). Right) High speed camera snapshots of a jetting and impact event. Snapshots 1–5 correspond to illustrations A-E.

Table 1
An overview of the dimensions and characteristics of the used chips (channel length, used channel filling levels, channel taper angle, orifice width and channel wall shape) and corresponding jet characteristics: diameter (D_{jet}), velocity (V_{jet}) and Weber number (We_{jet}).

Chip	Channel length	Filling levels	Taper angle	Orifice width	Channel wall	D_{jet}	V_{jet}	We_{jet}
1	1.9 mm	0.4–1.9 mm	7.5	50 μm	Flat	45–130 μm	7–37 m/s	70–2500
2	1.9 mm	0.9–1.9 mm	7.5	50 μm	Flat	40–110 μm	17–67 m/s	1200–4000
3	2.1 mm	0.7–1.9 mm	x	500 μm	Curved	35–100 μm	21–77 m/s	1600–4000

Table 2
Overview of the used test substrates (Borosilicate glass, and 2%, 1%, 0.5%, 0.25%, 0.125% agarose) and relevant characteristics: the Young's modulus and the Poisson's ratio that was used to calculate the shear modulus.

Substrate	E	υ	G
Glass	62.7 GPa	0.196	26.2 GPa
2% agarose	195.1 kPa	0.5	65 kPa
1% agarose	43.3 kPa	0.5	14 kPa
0.5% agarose	10.6 kPa	0.5	3.5 kPa
0.25% agarose	2.4 kPa	0.5	0.8 kPa
0.125% agarose	0.6 kPa	0.5	0.2 kPa

regimes, and characterized them in terms of the Weber-number of the impacting jet (We_{jet}) and substrate G. As We_{jet} describes the relative contribution of the fluid's inertia compared to the surface tension, it is often used to determine splashing thresholds of impacting liquids [38–40,54].

For these studies We_{jet} is defined as:

$$We_{jet} = \frac{(\rho V_{jet}^2 D_{jet})}{\sigma} \quad (1)$$

where ρ is the fluid density, V_{jet} is the jet velocity, D_{jet} is the jet diameter, and σ is the surface tension. In these experiments, both ρ and σ are constant, so We_{jet} is a function of V_{jet} and D_{jet}.

First, the seven regimes will be reviewed using illustrations for a clearer overview of the most important observations. More detailed figures composed of snapshots are provided, and movies of all regimes are found in the Supplementary Materials. Next, all regimes are combined into a regime map, and the the relation between We_{jet} and substrate G is discussed. For epidermal delivery, 1% and 2% agarose are most representative to bulk-skin stiffness (≈ 20 kPa) [24,27,26]. Additionally, studying impact on glass slides and lower agarose concentrations serves the purpose of exploring fundamental fluid dynamics and gaining insights on the splashing mechanisms. Finally, we review how the jet velocity and substrate stiffness relate to injection depth.

3.1. Regime 1: Jet spreading

In this regime, the jet spreads radially on the surface upon impact without splashing or deforming the substrate. Found for impact on glass (G = 26 GPa, $We_{jet} < 1150$) and 2% agarose (G = 65 kPa, $We_{jet} < 1290$), depicted in Fig. 2, top, and Supplementary Fig. 2). Impact duration depends on ejected volume, D_{jet} and V_{jet}, and lasts for 500 μs on average. The jet spreads on the surface upon impact, creating a smooth film that spreads radially over the surface and flows with wave formation. This is comparable to the deposition behavior described for droplets and macro-scale jets impacting solids [54,63]. As impact progresses, the amplitude of the waves increases and lamella formation is seen, sometimes to the point where asymmetric fingering edge formation can be seen, but no secondary droplets detach from the expanding liquid sheet. Asymmetric fingering is observed due to the chain oscillations [64], and intrinsic asymmetry of the impacting jet. This fingering behavior shows similarities to the fingering and subsequent droplet break-up reported for skating thin films on solid surfaces [65]. At the end of impact the film flow shows a decrease in frequency and amplitude of waves.

3.2. Regime 2: Jet splashing

Here, the jet splashes after it impacts the surface and no substrate deformation is seen. Found for impact on glass (G = 26 GPa, $We_{jet} > 1340$) and 2% agarose (G = 65 kPa, $We_{jet} > 1390$), and illustrated in Fig. 2, middle. Almost directly upon impact (Fig. 3, top), outward splashing is seen. At $We_{jet} < 3500$, liquid-film expansion occurs similarly to what has been described for Regime 1 (Fig. 3, bottom), whereas at $We_{jet} > 3500$ fingering and subsequent droplet release is seen. This indicates that for $We_{jet} > 3500$ the jet-tail has sufficient inertia to create secondary splashing within the liquid pool formed by the jet after impact, while jets impacting at $We_{jet} < 3500$ lack inertia, causing only outward splashing upon impact. In accordance with the findings of

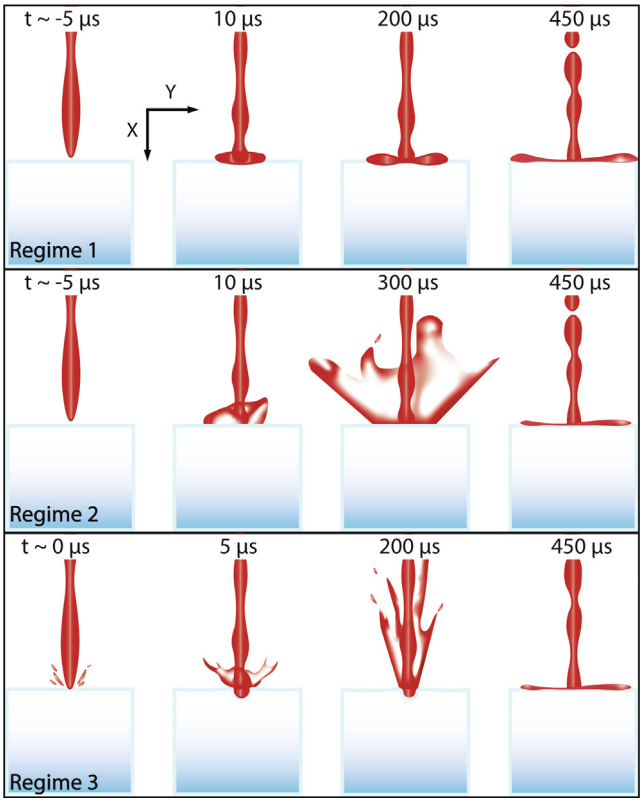

Fig. 2. Diagrams showing elastic substrate deformation regimes. Regime 1) Jet spreading: the jet impacts the substrate without visible deformation. The jet spreads and forms a pool without splashing. This regime is observed for G = 26 GPa, We_{jet} <1150 and G = 65 kPa, We_{jet} <1290. Regime 2) Jet splashing: the liquid jet impacts the surface and is not deformed, the jet splashes. Observed for: G = 26 GPa, We_{jet} >1340 and G = 65 kPa, We_{jet} >1390. Regime 3) Surface defeat: the jet impacts, creates a dimple in the surface and splashes at an angle corresponding to the dimple geometry. Observed for: G = 65 kPa, We_{jet} >3335; G = 14 kPa, We_{jet} = 400–1970; G = 3.5 kPa, We_{jet} <1060 and G = 0.8 kPa, We_{jet} <170. Supplementary Movies 1–3 show examples of the corresponding regimes.

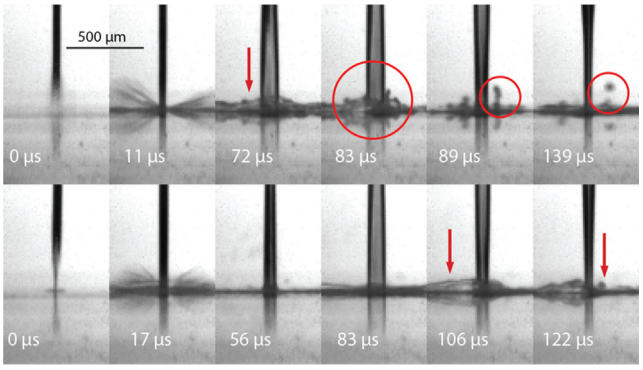

Fig. 3. Top) Jet double splashing upon glass. The jet splashes upon impact (t = 11 μs), and during impact a lamella forms (72 μs, red arrow), which starts to break-up (t = 83 μs, big red circle) and shows fingering (t = 89 μs, red arrow) resulting into secondary droplet release (139 μs, red circle). We_{jet} = 290 (V_{jet} = 16 m/s, D_{jet} = 55 μm). Supplementary Movie 4.1 shows the full event. Bottom) Jet single splashing. The jet splashes upon impact (t = 17 μs). During further impact lamella formation is seen (t = 106 μs, red arrow), which may cause some instabilities (t = 122 μs, red arrow) but does not result in secondary droplet release. We_{jet} = 130 (V_{jet} = 11 m/s, D_{jet} = 50 μm). See Supplementary Movie 4.2.

Howland et al., outward splashing occurred at lower We_{jet} for impact on glass as compared to agarose [40].

Splashing, the lamella formation and subsequent fingering can be described as follows. As the spreading front of the liquid rim advances, a lubrication force from the surrounding gas pushes the lamella upwards. If the lubrication force is larger than the surface tension the lamella will break up into secondary droplets [66]. Therefore the mean free path of the gas molecules (λ), the lamella thickness and speed determine the splashing phenomena.

For the splashing to happen, the lamella lift velocity has to be large enough to avoid the liquid to contact the solid again. Thus, the droplet will not splash if the rim diameter of the lamella increases faster than the lamella lifts from the substrate [53]. Thus, if the rim diameter of the lamella increases faster than the lamella lifts from the substrate, the droplet will not splash. Likewise, for micro-droplet impacts, the lamella thickness is in the order of magnitude of λ, making the airlift force negligible [51]. The threshold for inhibiting splashing was reported to be $We_\lambda = \rho\lambda V^2/\sigma \geqslant 0.5$, where $\lambda = 6.9 \times 10^{-5}$ m is the mean free path of the air at atmospheric pressure [51]. Qian et al. reported a jet splashing regime at We_{jet} = 617 (D_{jet} = 6 mm) [54], almost twice as low compared to our findings (We_{jet} = 1340). In contrast, Trainer et al. saw splashing of jets (D_{jet} = 3 mm) above We_{jet}= 1500 [67], closer to our findings. Therefore, we interpret that the low splashing threshold found by Qian et al. is due to the disturbances observed in the jets that lead to break-up [54].

3.3. Regime 3: Surface defeat

First, the jet splashes upon impact after which the impact creates elastic deformation in the surface and splashes at an angle corresponding to the deformation geometry. This regime is seen for impact on 2% agarose (G = 65 kPa, We_{jet} >3335), 1% agarose (G = 14 kPa, We_{jet} = 400–1970), 0.5% agarose (G = 3.5 kPa, We_{jet} <1060) and 0.25% agarose (G = 0.8 kPa, We_{jet} <170) and illustrated in Fig. 4, bottom. In detail, the jet splashes upon impact (t = 0 μs), as seen in regime 2, and subsequently creates a dimple in the substrate, followed by a secondary splash reaching heights > 750 μm. Uth et al. reported a similar situation for macro-jet (D_{jet} = 2 mm) impact on ceramics and gels [68], where the secondary splash is caused by back-flow. Indeed, upon impact, the jet creates a dimple with a depth ≈ 0.5 times D_{jet}, and flows back as it lacks force to further deform the surface. Additionally, the dimple geometry defines the back-flow angle, as reported earlier [68]. However, due to lack of resolution it is out of scope for these studies to give an exact relation. Finally, as impact progresses (t ≈ 400 μs), the dimple shrinks and disappears, while the final part of the jet impacts without splashing or injection.

3.4. Regime 4: Splash, injection and squeeze-out

Here, the jet splashes upon impacting the surface and injects into the substrate. However, once elastic recovery occurs, a portion of the injected liquid is squeezed-out of the substrate. This regime was found for 1% agarose (G = 14 kPa, We_{jet} < 2145), 0.5% agarose (G = 3.5 kPa, We_{jet}= 1240–3050) and 0.25% agarose (G = 0.8 kPa, We_{jet} <2145) and is depicted in Fig. 4, top. First, an initial dimple forms, followed by splashing that reaches heights of ≈ 750 μm), with an angle determined by the geometry of the dimple. As jet impact continues (t ≈ 200 μs), the dimple deepens and the substrate surface yields, causing the jet to penetrate further into the substrate while the splashing ceases. Uth et al. also found a decrease in splashing height along the injection duration [68].

Towards the end of the jet impact the injection depth no longer increases (t ≈ 400 μs). Liquid jets have a non-uniform velocity throughout the jet due to air resistance. This causes the jet tail to have a lower speed compared to its front, and consequently the

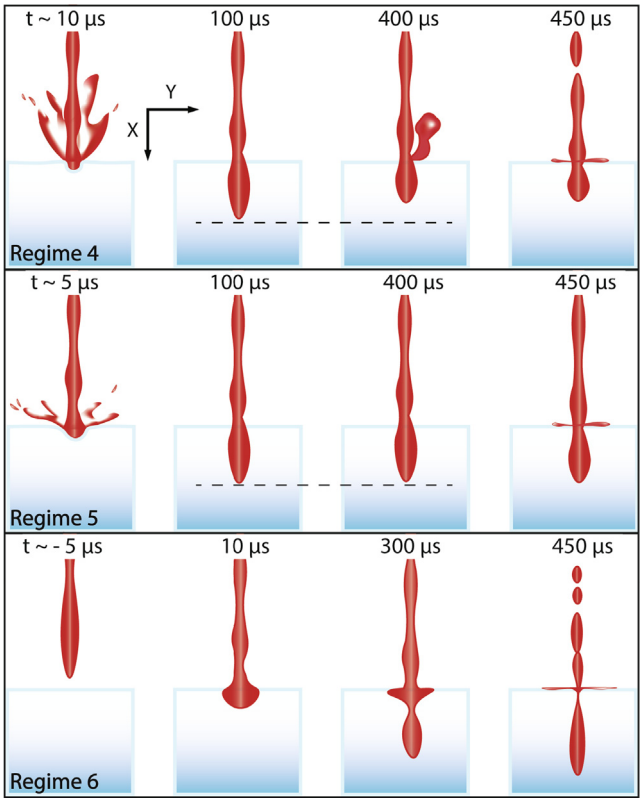

Fig. 4. Diagrams showing plastic substrate deformation regimes. Regime 4) Splash, injection and squeeze-out: The jet impact on the agarose gel surface creates a dimple and eventually penetrates the surface. Before penetrating, the jet splashes similarly to the surface defeat regime. After the injection, part of the injected liquid is expelled because of the visco-elastic properties of the gel. This regime is observed for: G = 14 kPa, $We_{jet} < 2145$; G = 3.5 kPa, We_{jet} = 1240–3050) and G = 0.8 kPa, $We_{jet} < 1240$. Regime 5) Splash and injection: This regime resembles Regime 4 in the first stages; there is jet splashing upon impact, and a dimple is formed and penetrated, but no liquid is expelled at the end of the process. This regime is observed for: G = 35 kPa, $We_{jet} > 3375$ and G = 0.8 kPa, We_{jet} = 655–1240. Regime 6) Clean injection: The jet impacts, deforms the surface and penetrates it. In this regime the jet does not splash. This is the ideal situation for needle-free jet injection systems. This regime is observed for: G = 0.8 kPa, $We_{jet} > 3375$ and G = 0.2 kPa, $We_{jet} < 270$. Supplementary Movies 4–6 show examples of the corresponding regimes.

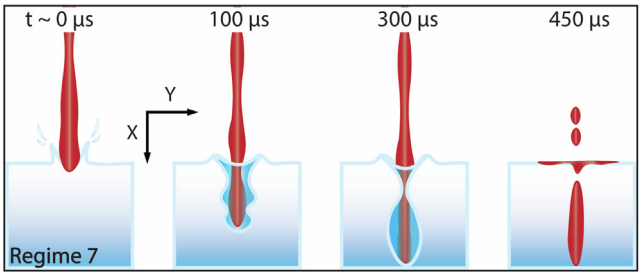

Fig. 5. Regime 7) Splashing Substrate: In this regime, the jet does not splash upon impact, but the substrate does. This regime was found only for: G = 0.2 kPa, $We_{jet} <$ 290. Supplementary Movies 7.1–7.2 show examples of the described regime.

impact pressure of the jet decreases over time. Moreover, agarose is a viscoelastic material [69], and its viscous response suppresses the elastic component temporarily during impact, allowing jet penetration. Once the elastic recovery occurs, as the jet impact force stagnates towards the end of the injection (t ≈ 400 μs), the gel returns to its original position, thereby squeezing out the liquid that penetrated the gel [70]. Due to limited optical resolution (1 pixel = 10 μm), it is out of scope of this paper to quantify the delivery efficiency. Furthermore, several papers have related the efficiency of the injection in terms of the percentage of jet volume loss and the injection strength ($S = (\rho V_{jet})/2G$) [71–73,18,15,33]. This loss is mainly due to splashing and squeeze out, however the detailed mechanism of the latter processes in needle-free injections lack attention.

3.5. Regime 5: Splash and injection

This regime resembles Regime 4, there is jet splashing upon impact, and a dimple is formed and penetrated, but no liquid is expelled after elastic recovery. Regime 5 (Fig. 4, middle), was found for impact on 0.5% agarose (G = 3.5 kPa, $We_{jet} > 3375$) and 0.25% agarose (G = 0.8 kPa, We_{jet} = 655–1240). First, a dimple is formed with minor splashing (50 – 100 μm), followed by substrate penetration. For agarose concentrations lower than 0.25% injection is seen at lower velocities (V_{jet} >30 m/s) as compared to the agarose concentrations (> 0.25%) $V_{jet} >$ 55 m/s. Since inter-molecular forces are larger for higher agarose concentrations [74,69,70], jet impact deforms the substrate instead of producing a splashing sheet. Towards the end of impact (t ≈ 400 μs), the injected area may compress or recede, but no squeeze-out is seen in contrast to Regime 4. Thus, in this regime we expect to reach the plastic deformation of the material, i.e., jet inertia overcomes the elasticity of the material beyond the recovery point. Additionally, while the jet penetrates (t ≈ 400–600 μs), the dimple in the surface flattens and widens, eventually pinching off from the injection cavity, sealing the injectate within the gel.

We can compare our results by looking at studies where high-speed projectiles were impacted on various concentrations of gelatin gels, and cavity regimes were defined based on projectile elastic Froude number (Fr_e) as function of substrate G [75], here, $Fr_e = (\rho V_{jet}^2)/G$. Within the reported cavity types our observations can be best compared to the shallow seal regime, which we found for G = 3.5 kPa and $We_{jet} > 3500$, $Fr_e > 1200$; G = 0.8 kPa and $We_{jet} > 650$, $Fr_e > 1000$; G = 0.2 kPa and We_{jet} = 125–215, $Fr_e >$ 700–1300. Our results are in agreement with Kiyama et al., where they found shallow seals starting from $Fr_e = 200 - 400$ and transitioning to surface seal at $Fr_e > 10^4$ [75]. We did not observe a transition to a surface seal as for our experiments $Fr_e < 10^4$.

3.6. Regime 6: Clean injection

The jet impacts, deforms the surface and penetrates it, without splashing at any stage (Fig. 3, bottom). This can be considered the optimal impact outcome or endpoint for needle-free injections. Observed for impacts on 0.25% agarose (G = 0.8 kPa, $We_{jet} >$ 3375) and 0.125% agarose (G = 0.2 kPa, $We_{jet} < 270$). In contrast to Regime 5, no splashing is seen because the jet-impact pressure only deforms the substrate. Compared to Regime 5, the dimple expands faster and wider (200 μs, 20–40 times D_{jet} for Regime 6 versus 400 μs, 1.5–2 times D_{jet} for Regime 5).

Observing at an angle (~ 45 degrees), different phases in the cavity dynamics can be highlighted (see Supplementary Fig. 3). First, the jet front forms a shallow dimple which expands into a bell-shaped cavity. The formation of cavities wider than D_{jet} is caused by pressure build-up of the impacting jet at the interface via momentum transfer from the jet, causing the pressure to move radially outwards and entraining the surrounding air [75]. Subsequently, the trailing part of the jet penetrates the gel surface forming a narrow secondary cavity, which finally seals the jet within the gel. For 0.25% agarose, the cavity-diameter is approxiamtely 20 times D_{jet}, whereas in 0.125% the cavity-diameter is around

40 times D_{jet} (t = 258 μs). Although these results showcase the optimal outcome for needle-free injections (e.g., no splash-back and 100 % delivery efficiency) we are aware that these simplified agarose gels provide a limited representation of the complexity of skin. Further investigations should be aimed at clarifying whether this outcome could be achieved with *in vivo* skin samples. However, this optimal scenario has been reported for *ex vivo* skin with $G = 0.3$ MPa and jet diameter and velocity $D_{jet} = 152$ μm, $V_{jet} = 159$ m/s [33].

3.7. Regime 7: Splashing substrate (no jet splashing)

The substrate splashes upon jet-impact, similarly to water entry experiments, i.e., secondary droplets detach from the substrate. Here, we note no jet splashing (see Fig. 4), with impact evolution similar to regime 6. This was the case for the softest substrate 0.125% agarose (G = 0.2 kPa) at $We_{jet} < 290$. For comparison, in water entry experiments this regime has been observed at $We \approx$ 180–230 [27,76].

As the jet starts penetrating the gel, the gel surface bulges (see Supplementary Fig. 3), and we observe a crown formation of the agarose sheet from where droplets detach. This crown formation resembles water entry experiments. However, higher *We* is required to obtain crown formation in agarose gels as compared to water. This was expected as viscous dissipation is larger in agarose gels than in water, and viscous dissipation stabilizes the crown rim [41,77]. Furthermore, agarose has a larger effective surface tension than water, and deviatoric stresses may also contribute to the higher impact speed leading to crown formation [77,78]. However, the former explanation is more plausible as the effective surface tension model from [77] has been shown useful to predict the penetration of a liquid jet through agarose gels with G ≈ 200 Pa [79].

As jet-impact progresses, the substrate-splashing ceases while the bulge remains and widens. At the end of the impact, the surface recovers to its original position. The bulging substrate-surface results from pressure build-up and momentum transfer from the impacting jet. Besides the substrate splashing upon jet-impact and the bulging surface, the injection and cavity dynamics are very similar to Regime 6.

3.8. Regime map

In Fig. 6 we show a regime map by plotting We_{jet}, in terms of the substrate shear modulus on a log–log scale. The blurred symbols represent the experimental data, and the larger symbols show the first transition value to a new regime. Both the transition from spreading to splashing and the transitions to different regimes show linear trends and we have derived three thresholds, defined as: spreading/splashing threshold: $We_{jet} = 299 \times G^{-0.047}(y_1)$; dimple formation threshold: $We_{jet} = 0.017 \times G^{1.1}(y_2)$; and plastic/elastic deformation threshold: $We_{jet} = 0.728 \times G^{0.83}(y_3)$.

Equation y1 indicates an increased splashing threshold for lower substrate stiffness, which was expected and reported by Howland et al. [40]. Furthermore, y2 allows calculating the required We_{jet} for dimple formation in substrates with known G. Doing so for G = 0.2 kPa, we find: We_{jet} = 6, indicating that all the generated jets within our experimental conditions would cause dimple formation on such substrates. Finally, y3 allows estimating the required We_{jet} to cause plastic deformation in materials with varying G. For a 40 μm jet diameter to create plastic deformation and inject into substrates of G = 65 kPa (2% agarose), V_{jet} should > 92 m/s. Furthermore, to create elastic deformation for G = 0.2 kPa (0.125% agarose) this corresponds to $We_{jet} < 60$, which would give V_{jet} = 8.3 m/s for D_{jet} = 40 μm. Unfortunately, verifying this experimentally would involve exploring new chip designs, to expand the jet velocity range, which is out of scope for this paper.

Baxter et al., studied jet delivery efficiency in skin samples with different stiffness, which can be used to compare our findings [33]. For We_{jet} = 53000 and G = 500 kPa [80,81], they report 6% delivery efficiency, indicating a high rate of elastic material response and little deformation, i.e., close to the threshold of elastic/plastic deformation. Evaluating equation y3 for G = 0.5 MPa, gives We_{jet} = 39100 as a threshold value for plastic deformation, which is ≈ 25% lower than 53000. Furthermore, for We_{jet} = 53000 the storage modulus at the threshold is G = 0.72 MPa, which in the same order of magnitude of the stiffest skin sample they injected (G = 0.96 MPa, wich gives: We_{jet} = 67000). Thus, our model matches Baxter et al. observations on the skin, validating our findings for a larger range of materials.

3.9. Comparison to skin impact

During these studies the glass plates and agarose concentrations 0.25 and 0.125% served to explore fundamental microfluidic jet impact dynamics while simultaneously gaining insights into the splashing behavior. The mechanical response of skin depends on multiple factors, and obtaining stiffness values relevant to our specific impact conditions is out of scope for these studies. To compare the regimes found in agarose and glass to the *in vivo* situation, some experimental conditions have been repeated using human skin as substrate (purchased via Biopredic International). The opaque nature of skin makes it impossible to validly define the threshold between regimes, as events happening within the substrate cannot be seen. Consequently, the transition between Regime 2 and 3, and the onset of dimple formation cannot be defined. Additionally, it is difficult to pinpoint the transition between regime 3 and 4, as it is hard to distinguish between pool filament splashing and squeeze-out, without tracking the back-flow inside the substrate, as shown in *Fig. 7*. However, based on the timing, duration and amplitude of splashing the phenomena in skin can be compared qualitatively to that on agarose gels. Doing so, splashing behaviour that could be caused by back-flow is indicated using red arrows, and potential squeeze-out is indicated using red circles in *Fig. 7*. Note that these observations remain qualitative based on comparable impact behaviour seen for the agarose gels. Additional experimental analysis and visualization of the flow inside the skin are required to distinguish between squeeze-out and filament splashing. Jets with $We_{jet} = 480 - 2600$ on human skin resulted in impact outcomes which are comparable to Regimes 1–3 (highlighted in Supplementary *Fig. 5*). Similarly, jets with $We_{jet} = 4000$ seem to result in Regime 4 as shown in *Fig. 7*. Within the capabilities of our experimental setup, the ideal Regime 6 (clean injection) could not be observed. Thus, new chips designs and set-up parameters should be explored to obtain jet with $We_{jet} > 53000$. Increasing We_{jet} will eventually lead to droplet break-up due to shear stress caused by the air, thereby posing a limitation to jet injection systems. However, previous works have not observed such breakup on generated jets with $D_{jet} = 15\mu$m and $V_{jet} \approx 1000$ m/s for injection on substrates with G 0.5 MPa *[15]*. The latter modulus lies within the reported modulus for skin *[24,80,81]*, indicating that increasing We_{jet} without observing breakup is possible. Furthermore, if needed, the use of surfactants or other additives can help stabilise the jets at higher We_{jet}.

Furthermore, as liquid properties also influence the impact behaviour, it should be assessed how the incorporation of therapeutics will affect splashing. The liquid characteristics used in these experiments closely match those of insulin used for therapy ($\eta \approx 1.1$ mPaS) [82]. In fact, most vaccines and other injectable therapeutics contain water-soluble ingredients, which results in

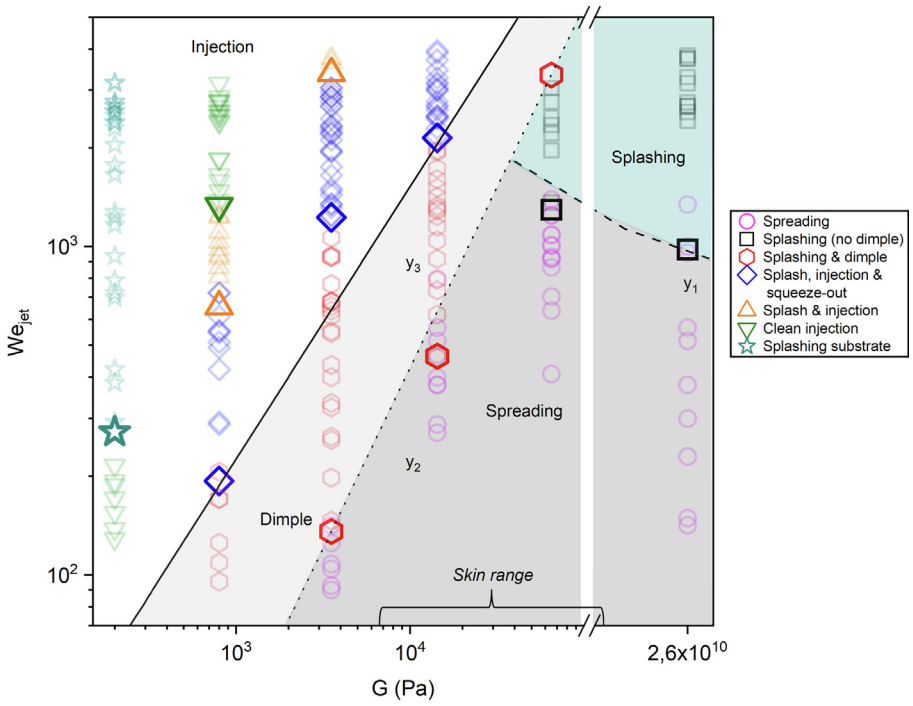

Fig. 6. Blurred symbols show all experimental conditions, while larger symbols indicate the first value at which a transition to a new regime was seen. The X-axis shows We_{jet} and the Y-axis shows substrate G in log–log scale. Symbol positions correspond to the substrates 0.125% agarose (G = 0.2 kPa), 0.25% agarose (G = 0.8 kPa), 0.5% agarose (G = 3.5 kPa), 1% agarose (G = 14 kPa), 2% agarose (G = 65 kPa) and borosilicate glass (G = 26 GPa). The dashed line ($y1 = 2993X^{-0.047}$) shows the spreading/splashing threshold*, the dotted line ($y2 = 0.017X^{1.1}$) shows the dimple formation threshold, and the solid line ($y3 = 0.728X^{0.83}$) shows the elastic/plastic deformation threshold. (The black brace indicates the reported range of skin stiffness (G = 6.6 kPa-333 MPa). Please note the axis break, emphasised by the narrow unmarked rectangle.

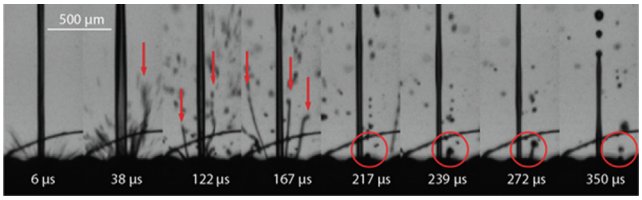

Fig. 7. Snapshots of jet impact at We_{jet}=4000 (V_{jet} = 61 m/s, D_{jet} = 50 μm) on skin in Regime 4. First, we observe outward splashing upon impact (t = 6 μs) followed by back-flow at times t = 38–167 μs, as indicated by the red arrows. From t = 217 μs (red circles) a small liquid filament rises from the skin surface, analogous to the squeeze-out behavior as described for agarose in Regime 4. The hair in the background, does not interact with the impacting jet as observed in Movie 11.

similar liquid properties [83]. Additionally, nanoparticle (NP) formulations have recently shown success in achieving enhanced pharmacokinetics and should therefore also be considered on compatibility with our system as NPs will be used in future therapies [84]. The effect of NPs on liquid properties depends on NP type and concentration. Lower splashing thresholds were reported for 45 nm Al_2O_3 NPs as it results in increased lamella spreading and lifting speed [85]. In contrast, for 10 nm $AgNO_3$ NPs splashing is suppressed at higher impact velocities because of interactions of the nanoparticles with the surface [86]. Therefore, we conclude that each NP based formulation needs to be separately studied to properly assess how the impact behaviour of the jets is influenced.

3.10. Injection depth dependency

The regimes we introduced in the previous section can assist in performing microfluidic jet injections where splash-back and partial ejection of the fluid is undesired. However, to further optimize our system, a reliable dependence of jet characteristics on injection depth (H_{inject}) in skin is needed. A linear relationship between V_{jet} and H_{inject} was previously reported [15,32,33]. In contrast, for We_{jet} and H_{inject}, there is no reported linear relationship. However, since the regimes we identified correlate with We_{jet}, it was also assessed how We_{jet} influences H_{inject}. We found that V_{jet} has a higher predictive value for H_{inject} as compared to We_{jet} (see Supplementary Fig. 7). The poor correlation coefficient of H_{inject} with We_{jet} is because We_{jet} depends on both D_{jet} and V_{jet}. Therefore, the same We_{jet} can result in jets with different V_{jet}. For example, a jet with D_{jet} four times larger than another jet, their velocity would be different by a factor of two.

To inject in substrates with G > 3.5 kPa, jets with high We_{jet} (> 2500), caused by high V_{jet} and low D_{jet}, are required to deform the surface. Such jets have a higher impact pressure due to their low surface area compared to high We_{jet}, resulting from average V_{jet}, yet high D_{jet}. Our observations align with previous studies of liquid jets impacting on liquid pools, where D_{jet} did not influence the final cavity depth, but the jet momentum did [87]. Therefore, we conclude that V_{jet} better predicts H_{inject} as compared to We_{jet}.

To gain more insight on the injection phenomena, we make an energy balance between the kinetic energy of the jet $E_k \sim V_{jet}^2 D_{jet}^2 H_{jet}$ (with H_{jet} the length of the jet) and $E_{el} \sim G D_{inject}^2 H_{inject}$ (where D_{inject} is the injection cavity diameter), the elastic energy of the cavity made in the agarose gel during the injection. Here, we assume that all the kinetic energy of the jet will be converted into elastic energy. Hence, by performing the energy balance and assuming that $D_{jet} \sim D_{inject}$ and that H_{jet} is constant in our experiments, we find that $H_{inject} \propto V_{jet}^2/G = Fr_e$. The linear relationship is in good agreement with the experimental data as shown in Fig. 8 Top.

Fig. 7, bottom, shows the evolution of the injection depth in time for different agarose concentrations. Prior to impact, V_{jet} =

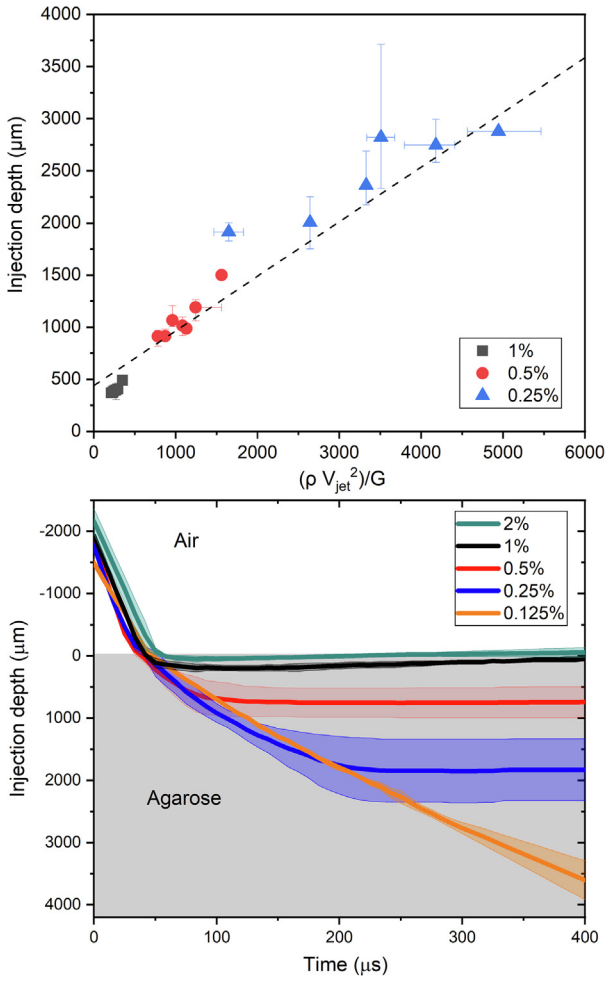

Fig. 8. Top) Relation between $(\rho V_{jet}^2)/G$ and H_{inject} for 1% agarose (G = 14 kPa), black; 0.5% agarose, red (G = 3.5 kPa) and 0.25% agarose (G = 0.8 kPa) Dashed line shows a linear fit ($y = 0.5243x + 440.04, R^2 = 0.935$). Bottom) Evolution of the injection depth in time for the different agarose gel concentrations ($V_{jet} \approx 58 \pm 11$ m/s, $We_{jet} = 3142 \pm 20\%$). The deceleration of the jet is greater for increasing agarose concentration. The solid lines indicate the average of 3 experiments, and the shaded area represents the variation across the experiments.

58 ± 11 m/s for all the experiments. The jet decelerates after impact onto the agarose gel surface. This deceleration increases with the concentration of agarose. For example, in agarose 2% the jet velocity in its traveling direction is 0 m/s as soon as it contacts the gel at t ~ 60 μs. In contrast, for agarose 0.125%, the velocity of the jet in the cavity is 1/2 V_{jet} remains almost constant until t ~ 400 μs. These results complement those on reference [18], where it was found that increasing the viscosity of the injected liquid while maintaining the other injection parameters constant, decreases the injection depth.

4. Conclusions

We studied the impact of microfluidic jets with a wide range of diameters (35–120 μm) and speeds (7–70 m/s), on substrates with a shear modulus between 0.2 kPa - 26 GPa. Microfluidic jets where created using a previously reported system envisioned for needle-free intradermal injections [11,2,5,27]. Seven distinct regimes were identified based on the jet Weber number (70–4000) and substrate stiffness: 1) Jet spreading, 2) Jet splashing, 3) Surface defeat, 4) Splash, injection and squeeze-out, 5) Splashing and injection, 6) Clean injection without splashing, and 7) splashing substrate (no jet splashing). Previous research focused on a narrower range of impact conditions and just reported two or three of the aforementioned regimes [40,68]. This is the first attempt to describe and report the seven different regimes in a single study, thus giving an extensive overview of phenomena that has been partially described [11,13,15,28,32].

Our findings enable calculating the thresholds between spreading and splashing, the threshold for dimple formation and the threshold between elastic and plastic material deformation. These thresholds can be used to predict the Weber number necessary to make a jet injection into a substrate of a known storage modulus. Moreover, we show qualitatively that the impact regimes observed in agarose gels and glass are similar to those observed for jet impact onto human *ex-vivo* skin. An empirical estimation of the threshold between regions could not be determined due to the opacity of skin. However, the threshold between elastic and plastic material deformation matched available data on injections onto *ex-vivo* skin [33]. This result is especially relevant for needle-free injections as skin storage modulus differs between people or regions of the body [23–25].

Additionally, understanding how jet Weber number relates to splashing and squeeze-out can help optimize liquid jet injections by reducing both phenomena, as they have been found to be a limitation to needle-free injection systems [36,37]. To enhance delivery efficiency and decrease infection risks, higher jet Weber number should be explored.

Furthermore, as reported previously [33], we found that jet velocity is a better predictor for the injection depth compared to the Weber number, especially for the higher agarose percentages, as the Weber number depends on both jet velocity and diameter. To deform substrates with G > 3.5 kPa, high impact pressure is required that is only provided by jets with high velocity and small diameter. By making an energy balance, we found that the injection depth $H_{inject} \sim Fr_e$, which is in good agreement with the experimental data.

Although agarose gels cover the same shear modulus range as skin, they lack the various elements of skin that confer its complex mechanical behaviour. Therefore further studies are needed to contrast our observations in agarose and glass against skin samples. Future work could also be aimed at increasing the range of jet velocities to expand the regime map, and verify to what extent our calculated thresholds have predictive value over skin samples with varying shear moduli.

Declaration of Competing Interest

The authors declare that they have no known competing financial interests or personal relationships that could have appeared to influence the work reported in this paper.

Acknowledgments

The authors acknowledge the funding from the European Research Council (ERC) under the European Union's Horizon 2020 Research and Innovation Programme (Grant Agreement No. 851630), and NWO Take-off phase 1 program funded by the Ministry of Education, Culture and Science of the Government of the Netherlands (No. 18844). The authors would like to thank J.J. Schoppink for both the contact angle measurements and discussions. The authors are thankful for the insightful discussions with K. Mohan and S. Schlautmann.

Appendix A. Supplementary material

Supplementary data associated with this article can be found, in the online version, at https://doi.org/10.1016/j.jcis.2023.01.024.

References

[1] World-Health-Organization, Safety of injections: Global facts and figures, https://www.who.int/teams/integrated-health-services/infection-prevention-control, accessed 15-04-2022.
[2] Bloomberg, The bloomberg covid-19 vaccine tracker, https://github.com/BloombergGraphics/covid-vaccine-tracker-data, accessed 12-06-2022.
[3] K. Padmanabhan and D. Barik, Energy from Toxic Organic Waste for Heat and Power Generation, edited by D. Barik, Woodhead Publishing Series in Energy (Woodhead Publishing, 2019) pp. 99–118
[4] M.C.M. Alvim-Ferraz, S.A.V. Afonso, Incineration of different types of medical wastes: Emission factors for particulate matter and heavy metals, Environ. Sci. Technol. 37 (2003) 3152.
[5] L.O. Alifariki, A. Kusnan, I.M.C. Asriati, S. Susanty Binekada, W.S. Sukurni, I.M. Afrini Hajri, Y. Syam, Safe injection practices and the incident of needle stick injuries (nsis), Enfermería Clínica 30 (2020) 73.
[6] A.M. Hauri, G.L. Armstrong, Y.J. Hutin, The global burden of disease attributable to contaminated injections given in health care settings, Int J STD AIDS15 7 (2004).
[7] S. Wright, M. Yelland, K. Heathcote, S.K. Ng, G. Wright, Fear of needles-nature and prevalence in general practice, Aust. Fam. Phys. 38 (2009) 172.
[8] T. Orenius, H. LicPsych, K. Mikola Säilä, L. Ristolainen, Fear of injections and needle phobia among children and adolescents: An overview of psychological, behavioral, and contextual factors, SAGE Open Nurs4 (2018).
[9] J. McLenon, M.A. Rogers, The fear of needles: A systematic review and meta-analysis, J. Adv. Nurs. 75 (2019) 30.
[10] A.S. Love, R.J. Love, Considering needle phobia among adult patients during mass covid-19 vaccinations, J. Primary Care Commun. Health 12 (2021).
[11] J. Schoppink, D. Fernandez Rivas, Jet injectors: Perspectives for small volume delivery with lasers, Advanced, Drug Delivery Reviews 182 (2022).
[12] S. Mitragotri, Current status and future prospects of needle-free liquid jet injectors, Nat. Rev. Drug Discov. 5 (2006) 543.
[13] J. Baxter, S. Mitragotri, Needle-free liquid jet injections: mechanisms and applications, Expert Rev. Med. Devices 3 (2006) 565.
[14] J.R. Schramm-Baxter, S. Mitragotri, Investigations of needle-free jet injections, Conf. Proc. IEEE Eng. Med. Biol. Soc. 2004 (2004) 3543.
[15] J. Krizek, P. Delrot, and C. Moser, Repetitive regime of highly focused liquid microjets for needle-free injection, Scientific Reports10 (2020).
[16] A. Arora, I. Hakim, J. Baxter, R. Rathnasingham, R. Srinivasan, D.A. Fletcher, and S. Mitragotri, Needle-free delivery of macromolecules across the skin by nanoliter-volume pulsed microjets, Proc. Natl. Acad. Sci. 104, 4255 (2007).
[17] A.M. Römgens, D. Rem-Bronneberg, R. Kassies, M. Hijlkema, D.L. Bader, C.W.J. Oomens, M.P.B. van Bruggen, Penetration and delivery characteristics of repetitive microjet injection into the skin, J. Control. Release 234 (2016) 98.
[18] L.O. Gálvez, A. Fraters, H.L. Offerhaus, M. Versluis, I.W. Hunter, D.F. Rivas, Microfluidics control the ballistic energy of thermocavitation liquid jets for needle-free injections, J. Appl. Phys. 127 (2020) 104901.
[19] J. Gupta, S.S. Park, B. Bondy, E.I. Felner, M.R. Prausnitz, Infusion pressure and pain during microneedle injection into skin of human subjects, Biomaterials 32 (2011) 6823.
[20] G.M. Glenn, R.T. Kenney, Mass vaccination: solutions in the skin, Curr. Top Microbiol. Immunol. 304 (2006) 247.
[21] M.R. Prausnitz, R. Langer, Transdermal drug delivery, Nat. Biotechnol. 26 (2008) 1261.
[22] Y. Zhang, J. Yu, A.R. Kahkoska, J. Wang, J.B. Buse, Z. Gu, Advances in transdermal insulin delivery, Adv. Drug Deliv. Rev. 139 (2019) 51.
[23] M. Mercuri, D. Fernandez Rivas, Challenges and opportunities for small volumes delivery into the skin, Biomicrofluidics, 2021, 15.
[24] H.K. Graham, J.C. McConnell, G. Limbert, M.J. Sherratt, How stiff is skin?, Exp Dermatol. 28 (2019) 4.
[25] J. van Kuilenburg, M.A. Masen, E. van der Heide, Contact modelling of human skin: What value to use for the modulus of elasticity?, Proc Inst. Mech. Eng., Part J: J. Eng. Tribol. 227 (2012) 349.
[26] A. Kalra, A. Lowe, An overview of factors affecting the skins youngs modulus, J. Aging Sci. 4 (2016).
[27] C. Berrospe-Rodriguez, C.W. Visser, S. Schlautmann, D.F. Rivas, R. Ramos-Garcia, Toward jet injection by continuous-wave laser cavitation, J. Biomed. Opt. 22 (2017) 1.
[28] P. Rohilla, I. Lawal, A. Le Blanc, V. O'Brien, C. Weeks, W. Tran, Y. Rane, E. Khusnatdinov, J. Marston, Loading effects on the performance of needle-free jet injections in different skin models, J. Drug Deliv. Sci. Technol. 60 (2020).
[29] M.L. Crichton, X. Chen, H. Huang, M.A.F. Kendall, Elastic modulus and viscoelastic properties of full thickness skin characterised at micro scales, Biomaterials 34 (2013) 2087.
[30] H. Joodaki and M. Panzer, Skin mechanical properties and modeling: A review, Proceedings of the Institution of Mechanical Engineers, Part H: Journal of Engineering in Medicine232 (2018).
[31] S. Pan, D. Malhotra, N. Germann, Nonlinear viscoelastic properties of native male human skin and in vitro 3d reconstructed skin models under laos stress, J. Mech. Behav. Biomed. Mater. 96 (2019) 310.
[32] Y. Tagawa, N. Oudalov, A.E. Ghalbzouri, C. Sun, D. Lohse, Needle-free injection into skin and soft matter with highly focused microjets, Lab Chip 13 (2013) 1357.
[33] J. Baxter, S. Mitragotri, Jet-induced skin puncture and its impact on needle-free jet injections: Experimental studies and a predictive model, J. Controlled Release 106 (2005) 361.
[34] J. Schramm-Baxter, J. Katrencik, S. Mitragotri, Jet injection into polyacrylamide gels: investigation of jet injection mechanics, J. Biomech. 37 (2004) 1181.
[35] J.A. Simmons, J. Davis, J. Thomas, J. Lopez, A. Le Blanc, H. Allison, H. Slook, P. Lewis, J. Holtz, P. Fisher, K.E. Broderick, J.O. Marston, Characterization of skin blebs from intradermal jet injection: Ex-vivo studies, J. Controlled Release 307 (2019) 200.
[36] T. Gilet, L. Bourouiba, Fluid fragmentation shapes rain-induced foliar disease transmission, J. Roy. Soc. Interface 12 (2015) 20141092.
[37] P.H. Gregory, E.J. Guthrie, M.E. Bunce, Experiments on splash dispersal of fungus spores, Microbiology 20 (1959) 328.
[38] A. Yarin, Drop impact dynamics: Splashing, spreading, receding, bouncing, Annu. Rev. Fluid Mech. 38 (2006) 159.
[39] C. Josserand, S. Thoroddsen, Drop impact on a solid surface, Annu. Rev. Fluid Mech. 48 (2016) 365.
[40] C.J. Howland, A. Antkowiak, J.R. Castrejón-Pita, S.D. Howison, J.M. Oliver, R.W. Style, A.A. Castrejón-Pita, It's harder to splash on soft solids, Phys. Rev. Lett. 117 (2016).
[41] A. Mohammad Karim, Experimental dynamics of newtonian and non-newtonian droplets impacting liquid surface with different rheology, Phys. Fluids, 32 (2020).
[42] E.J. Vega, A.A. Castrejón-Pita, Suppressing prompt splash with polymer additives, Exp. Fluids 58 (2017) 57.
[43] J.M. López-Herrera, S. Popinet, A.A. Castrejón-Pita, An adaptive solver for viscoelastic incompressible two-phase problems applied to the study of the splashing of weakly viscoelastic droplets, J. Nonnewton. Fluid Mech. 264 (2019) 144.
[44] M.A. Quetzeri-Santiago, A.A. Castrejón-Pita, J.R. Castrejón-Pita, The effect of surface roughness on the contact line and splashing dynamics of impacting droplets, Scient. Rep., 9, 2019a.
[45] D.G.K. Aboud, A.-M. Kietzig, Splashing threshold of oblique droplet impacts on surfaces of various wettability, Langmuir 31 (2015) 10100.
[46] M. Quetzeri-Santiago, K. Yokoi, A. Castrejón-Pita, R. Castrejon-Pita, Role of the dynamic contact angle on splashing, Phys. Rev. Lett. 122 (2019), https://doi.org/10.1103/PhysRevLett.122.228001.
[47] J. Hao, Effect of surface roughness on droplet splashing, Phys. Fluids 29 (2017) 122105.
[48] W. Bouwhuis, X. Huang, C. Chan, P.E. Frommhold, C.-D. Ohl, D. Lohse, J.H. Snoeijer, D. van der Meer, Impact of a high-speed train of microdrops on a liquid pool, J. Fluid Mech. 792 (2016) 850.
[49] S. Mandre, M.P. Brenner, The mechanism of a splash on a dry solid surface, J. Fluid Mech. 690 (2012) 148.
[50] T.C. Sykes, B.D. Fudge, M.A. Quetzeri-Santiago, J.R. Castrejón-Pita, A.A. Castrejón-Pita, Droplet splashing on curved substrates, J. Colloid Interface Sci. 615 (2022) 227.
[51] M. Usawa, Y. Fujita, Y. Tagawa, G. Riboux, J.M. Gordillo, Large impact velocities suppress the splashing of micron-sized droplets, Physical Review Fluids 6 (2021).
[52] C.W. Visser, Y. Tagawa, C. Sun, D. Lohse, Microdroplet impact at very high velocity, Soft Matter 8 (2012) 10732.
[53] C.W. Visser, P.E. Frommhold, S. Wildeman, R. Mettin, D. Lohse, C. Sun, Dynamics of high-speed micro-drop impact: numerical simulations and experiments at frame-to-frame times below 100 ns, Soft Matter 11 (2015) 1708.
[54] S. Qian, D.Z. Zhu, H. Xu, Splashing generation by water jet impinging on a horizontal plate, Exp. Thermal Fluid Sci. 130 (2022).
[55] N.B. Speirs, Z. Pan, J. Belden, T.T. Truscott, The water entry of multi-droplet streams and jets, J. Fluid Mech. 844 (2018) 1084.
[56] H.M. Kittel, E. Alam, I.V. Roisman, C. Tropea, T. Gambaryan-Roisman, Splashing of a newtonian drop impacted onto a solid substrate coated by a thin soft layer, Colloids Surf., A 553 (2018) 89.
[57] B.C. Basso, J.B. Bostwick, Splashing on soft elastic substrates, Langmuir 36 (2020) 15010.
[58] S.F. Rastopov and A.T. Sukhodolsky, Optical Radiation Interaction with Matter (Proceedings of Spie, 1991)
[59] J.P. Padilla-Martinez, C. Berrospe-Rodriguez, G. Aguilar, J.C. Ramirez-San-Juan, and R. Ramos-Garcia, Optic cavitation with cw lasers: A review, Physics of Fluids26 (2014).
[60] A. Antkowiak, N. Bremond, S. Le DizÈS, E. Villermaux, Short-term dynamics of a density interface following an impact, J. Fluid Mech. 577 (2007) 241.
[61] F. Scheaua, Theoretical approaches regarding the venturi effect, HIDRAULICA - Magazine of Hydraulics, Pneumatics, Tribology, Ecology, Sensorics, Mechatronics III 69 (2016).
[62] G. Paltauf, P.E. Dyer, Photomechanical processes and effects in ablation, Chem. Rev. 103 (2003) 487.
[63] R. Rioboo, M. Marengo, C. Tropea, Outcomes from a drop impact on solid surfaces, ATOMIZATION AND SPRAYS 11 (2001) 155.

[64] D.T.A. Jordan, N.M. Ribe, A. Deblais, D. Bonn, Chain oscillations in liquid jets, Physical Review Fluids 7 (2022) 104001.
[65] M.M. Driscoll, S.R. Nagel, Ultrafast interference imaging of air in splashing dynamics, Phys. Rev. Lett. 107 (2011) 154502.
[66] G. Riboux, J.M. Gordillo, Experiments of drops impacting a smooth solid surface: A model of the critical impact speed for drop splashing, Phys. Rev. Lett. 113 (2014).
[67] D. Trainer, Breakup length and liquid splatter characteristics of air-assisted water jets, Int. J. Multiph. Flow 81 (2016), https://doi.org/10.1016/j.ijmultiphaseflow.2016.02.005.
[68] T. Uth and V.S. Deshpande, Unsteady penetration of a target by a liquid jet, Proceedings of the National Academy of Sciences 110, 20028 (2013).
[69] A. Ed-Daoui, M. Benelmostafa, and M. Dahmani, Study of the viscoelastic properties of the agarose gel, Materials Today: Proceedings 13, 746 (2019).
[70] M. Salerno, S. Dante, N. Patra, A. Diaspro, Afm measurement of the stiffness of layers of agarose gel patterned with polylysine, Microsc. Res. Tech. 73 (2010) 982.
[71] K. Cu, R. Bansal, S. Mitragotri, D. Fernandez Rivas, Delivery strategies for skin: comparison of nanoliter jets, needles and topical solutions, Annals of biomedical engineering48 48 (2020) 2028.
[72] L. Oyarte Galvez, M. Brio Perez, D. Fernandez Rivas, High speed imaging of solid needle and liquid micro-jet injections, Journal of applied physics 125 (2019) 144504.
[73] A.M. Römgens, D. Rem-Bronneberg, R. Kassies, M. Hijlkema, D.L. Bader, C.W. Oomens, M.P. van Bruggen, Penetration and delivery characteristics of repetitive microjet injection into the skin, Journal of controlled release234 (2016) 98.
[74] V. Normand, D.L. Lootens, E. Amici, K.P. Plucknett, P. Aymard, New insight into agarose gel mechanical properties, Biomacromolecules 1 (2000) 730.
[75] A. Kiyama, M.M. Mansoor, N.B. Speirs, Y. Tagawa, T.T. Truscott, Gelatine cavity dynamics of high-speed sphere impact, J. Fluid Mech. 880 (2019) 707.
[76] Schott, noop Technical details of mempax borosilicate glass, https://www.schott.com/en-my/products/mempax-p1000322/technical-details, accessed 15-04-2022.
[77] X. Shao, S.A. Fredericks, J.R. Saylor, J.B. Bostwick, A method for determining surface tension, viscosity, and elasticity of gels via ultrasonic levitation of gel drops, The Journal of the Acoustical Society of America 147 (2020) 2488.
[78] E. James, S. Tangparitkul, A. Brooker, C. Amador, A. Graydon, M. Vaccaro, O.J. Cayre, T.N. Hunter, D. Harbottle, Accelerated spreading of inviscid droplets prompted by the yielding of strongly elastic interfacial films, Colloids Surf., A 554 (2018) 326.
[79] M. Quetzeri-Santiago and D. Fernandez Rivas, Cavity dynamics after the injection of a microfluidic jet in capillary bridges (2022).
[80] C. Li, G. Guan, R. Reif, Z. Huang, R.K. Wang, Determining elastic properties of skin by measuring surface waves from an impulse mechanical stimulus using phase-sensitive optical coherence tomography, J R Soc Interface 9 (2012) 831.
[81] T.R. Tilleman, M.M. Tilleman, M.H. Neumann, The elastic properties of cancerous skin: Poisson's ratio and young's modulus, Isr Med Assoc J6 (2004) 753.
[82] G.G. Adams, A. Meal, P.S. Morgan, Q.E. Alzahrani, H. Zobel, R. Lithgo, M.S. Kok, D.T. Besong, S.I. Jiwani, S. Ballance, et al., Characterisation of insulin analogues therapeutically available to patients, PLoS One13 e0195010 (2018).
[83] S.-S. Wong, R.J. Webby, Traditional and new influenza vaccines, Clinical microbiology reviews 26 (2013) 476.
[84] S. Soares, J. Sousa, A. Pais, and C. Vitorino, Nanomedicine: Principles, properties, and regulatory issues, Frontiers in Chemistry 6, DOI: 10.3389/fchem.2018.00360 (2018).
[85] Y.T. Aksoy, P. Eneren, E. Koos, M.R. Vetrano, Spreading-splashing transition of nanofluid droplets on a smooth flat surface, J. Colloid Interface Sci. 606 (2022) 434.
[86] M.-J. Thoraval, J. Schubert, S. Karpitschka, M. Chanana, F. Boyer, E. Sandoval-Naval, J.F. Dijksman, J.H. Snoeijer, D. Lohse, Nanoscopic interactions of colloidal particles can suppress millimetre drop splashing, Soft Matter 17 (2021) 5116.
[87] T. Kroeze, Direct numerical simulations of microfluidic jets, University of Twente, The Netherlands, 2022. Master Thesis.